Available online at www.sciencedirect.com
SCIENCE DIRECT®
ELSEVIER
Journal of Magnetism and Magnetic Materials 294 (2005) 99–106
Journal of magnetism and magnetic materials
www.elsevier.com/locate/jmmm

Anisotropies in soft magnetic nanocrystalline alloys

Giselher Herzer*

Vacuumschmelze GmbH & Co. KG, Grüner Weg 37, D-63450 Hanau, Germany

Available online 2 May 2005

Abstract

The article reviews and updates the understanding of the soft magnetic properties of nanocrystalline Fe-based alloys. In optimized compositions the random magneto-crystalline anisotropy of the structural phases is largely averaged out. The soft magnetic properties are then controlled by magneto-elastic and induced anisotropies which are uniform on a scale much larger than the exchange length. But unlike to the case of soft magnetic amorphous alloys, there is still a competition between the random and the more uniform anisotropy contributions. The experimental findings are complemented by theoretical results.

PACS: 75.30.Gw; 75.60.−d; 75.75+a

Keywords: Random anisotropy; Induced anisotropy; Exchange length; Grain size dependence of coercivity and permeability; Nanocrystalline Fe-based alloys

1. Introduction

Nanocrystalline Fe–Cu–Nb–Si–B alloys (cf. [1–3]) reveal a homogeneous ultrafine grain structure of BCC FeSi with grain sizes D of typically 10–15 nm and random orientation, embedded in an amorphous minority matrix. This particular microstructure is obtained by devitrification from the amorphous state and enables excellent soft magnetic properties comparable to those of permalloys and Co-based amorphous alloys. Optimized alloy compositions like $Fe_{73}Cu_1Nb_3Si_{16}B_7$ moreover reveal near-zero saturation magnetostriction ($|\lambda_s| < 0.2$ ppm) and meanwhile have successfully entered into application under the trademarks FINEMET FT-3® [4] or VITROPERM® 800 [5,6].

The article discusses the anisotropy contributions relevant for the soft magnetic properties of these materials.

2. Random anisotropies

The microstructure leads to a distribution of magnetic anisotropy axis randomly varying their orientation over the scale of the grain size D. The soft magnetic properties basically arise from the

*Tel./fax: +49 6181 38 3002.
E-mail address: giselher.herzer@vacuumschmelze.com.

0304-8853/$ - see front matter © 2005 Elsevier B.V. All rights reserved.
doi:10.1016/j.jmmm.2005.03.020

suppression of these local random anisotropies by exchange interaction [2] similar to the case of amorphous metals [7]. The mechanism becomes effective for grain sizes, D, smaller than the basic ferromagnetic exchange length,

$$L_0 = \varphi_0 \sqrt{A/|K_1|}, \quad (1)$$

where A is the exchange stiffness, K_1 is the local magnetic anisotropy constant and φ_0 is a proportionality factor in the order of one. L_0 represents a characteristic minimum scale below which the direction of the magnetization cannot vary appreciably. It, for example, determines the order of the domain wall width for $D > L_0$. Typical values are $L_0 \approx 5$–10 nm for Co-based and $L_0 \approx 20$–40 nm for Fe-based alloys. Thus, both amorphous ($D \approx$ atomic scale) and nanocrystalline alloys ($D \approx 5$–20 nm) fall into the regime $D < L_0$ where the smoothing action of exchange energy impedes the magnetization to follow the random orientations of the local anisotropy axis. As a consequence the local anisotropies are largely washed out and the average anisotropy constant $\langle K_1 \rangle$ scales down as [2,3]

$$\langle K_1 \rangle = |K_1| \cdot x^2 (D/L_0)^6, \quad (2)$$

where x denotes the crystalline volume fraction. As shown in Fig. 1, this behavior is well reflected in the grain size dependence of coercivity H_c ($\propto \langle K_1 \rangle$) and permeability μ ($\propto 1/\langle K_1 \rangle$).

The experimental data in Fig. 1 reveal a relatively broad scatter. The reason is that the experimental variation of the grain size cannot be performed in a completely straight forward way. It inevitably requires changes of the alloy composition and/or the annealing conditions. Both changes the volume fraction and composition of the crystallites and the residual matrix. As a consequence the local magneto-crystalline anisotropy constant, K_1, and the exchange interaction, A, between the grains change simultaneously.

Nonetheless, the grain size dependence in Eq. (2) provides a good guiding principal through most of the data. However, there are also systematic deviations from the theoretical D^6 dependence due to

1. additional crystalline phases and/or
2. magneto-elastic and induced anisotropies.

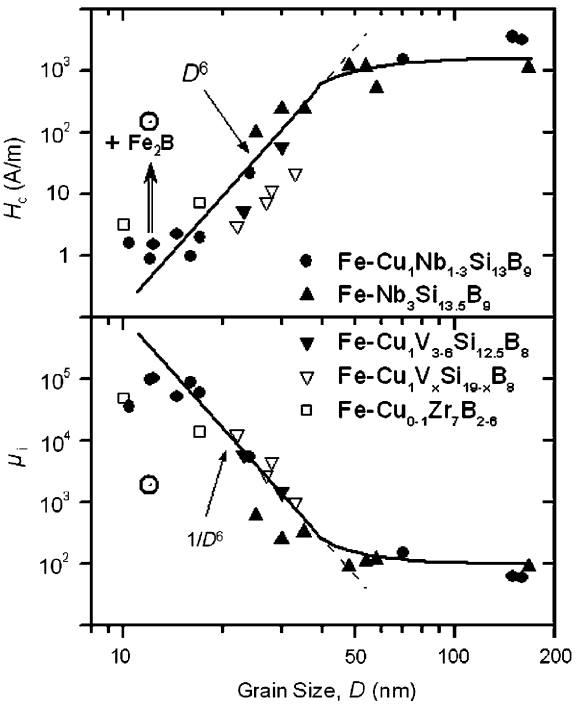

Fig. 1. Coercivity H_c and initial permeability μ_i of Fe-based nanocrystalline alloys as a function of the average grain size D (cf. [3]). The open circle corresponds to an "overannealed" $Fe_{73.5}Cu_1Nb_3Si_{13.5}B_9$ alloy with a small fraction (less than 10%) of Fe_2B precipitates.

Thus, the precipitation of small fractions of Fe_2B compounds can drastically affect the soft magnetic properties although the grain size of the BCC crystallites may remains unchanged (cf. Fig. 1). This is due to the huge magneto-crystalline anisotropy constant of Fe_2B ($K_1(Fe_2B) = -430\,kJ/m^3$) which is almost two orders of magnitude larger than that of the FeSi grains ($K_1(Fe_{80}Si_{20}) = 8.2\,kJ/m^3$). Accordingly, the good soft magnetic properties of the nanocrystalline BCC structure are largely recovered at 250 °C where $K_1(Fe_2B)$ passes through zero (cf. [3]).

Magneto-elastic and induced anisotropies lead to a vanishing or modified grain size dependence of coercivity and permeability at grain sizes below about 15–20 nm. Suzuki et al. [8] report a $H_c \propto D^3$ law for nanocrystalline $Fe_{91}Zr_7B_2$, while H_c appears to be approximately constant at small grain sizes for Fe–Cu–Nb–Si–B-type compositions (see also Fig. 1).

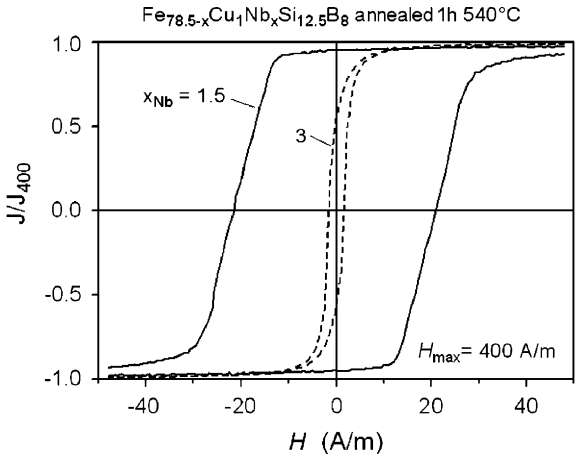

Fig. 2. Characteristic hysteresis loops in the nanocrystalline state. The average grain sizes for the examples shown are about 25 nm for $x_{Nb} = 1.5$ at% and 12 nm for $x_{Nb} = 3$ at%, respectively.

Fig. 2 shows some typical hysteresis loops for $D < L_0$. In the regime of the D^6 law, the hysteresis loops reveal a high remanence to saturation ratio J_r/J_s. An example with $J_r/J_s \approx 0.95$ is given in Fig. 2 by the sample with $D \approx 25$ nm. Such a remanence enhancement towards $J_r/J_s = 1$ is another characteristic feature when exchange interaction starts to dominate over anisotropy. The phenomenon is of particular interest for tailoring isotropic, nanoscaled hard magnets (cf. [9]).

As also demonstrated in Fig. 2 (sample with $D = 12$ nm), the remanence ratio decreases to values around 0.5 shown at smaller grain sizes. This clearly indicates that the magnetization process is dominated by a distribution of uniaxial anisotropies which are uniform on a scale much larger than the exchange length. Wide regular domains as well as typical stress patterns found in corresponding samples [10] confirm this conclusion.

3. Uniform anisotropies

Indeed, it appears that, like in amorphous metals, the average random anisotropy of optimized nanocrystalline alloys is negligibly small and that the soft magnetic properties are predominantly controlled by uniaxial anisotropies which are uniform on a scale much larger than the exchange length. Relevant to this are magnetoelastic anisotropies, creep or field induced anisotropies and/or shape anisotropies originating from the sample geometry or surface roughness.

Thus, the ultimate reason for the good soft magnetic properties of nanocrystalline Fe-based alloys is that the formation of the nanocrystalline state can lead to a low or vanishing saturation magnetostriction (cf. [3]). This minimizes the contribution of magneto-elastic anisotropies due to internal mechanical stresses. Superior soft magnetic properties are, therefore, found for alloy compositions like $Fe_{bal.}Cu_1Nb_3Si_{12-17}B_{6-9}$ where magnetostriction is less than a few ppm or even zero for Si-contents around 16 at%.

So far, magnetic anisotropies have been discussed as a rather disturbing factor for soft magnetic properties. However, if properly controlled, they can be a powerful tool in order to tailor the shape of the hysteresis loop according to the demands of application. This is the particular case with field induced anisotropies.

Fig. 3 shows the hysteresis loops and the permeability of magnetic field annealed $Fe_{73.5-}Cu_1Nb_3Si_{13.5}B_9$. The almost perfect rectangular or linear hysteresis loops obtained after field annealing indicate that the induced anisotropy clearly dominates over magneto-elastic and magnetocrystalline anisotropies. Still, the induced anisotropy constant, K_u, can be tailored small enough in order to achieve highest permeabilities (cf. Fig. 3).

The *round* loop (R) shown in Fig. 3 results after annealing without magnetic field. This, however, does not mean that there are no induced anisotropies. The latter are always induced along the direction of the local spontaneous magnetization within a ferromagnetic domain. Thus, annealing without field simply produces a distribution of uniaxial anisotropies fluctuating on the micrometer scale of the domain pattern during annealing.

4. Competition of random and uniform anisotropies

Although the soft magnetic properties in optimized compositions are predominantly controlled

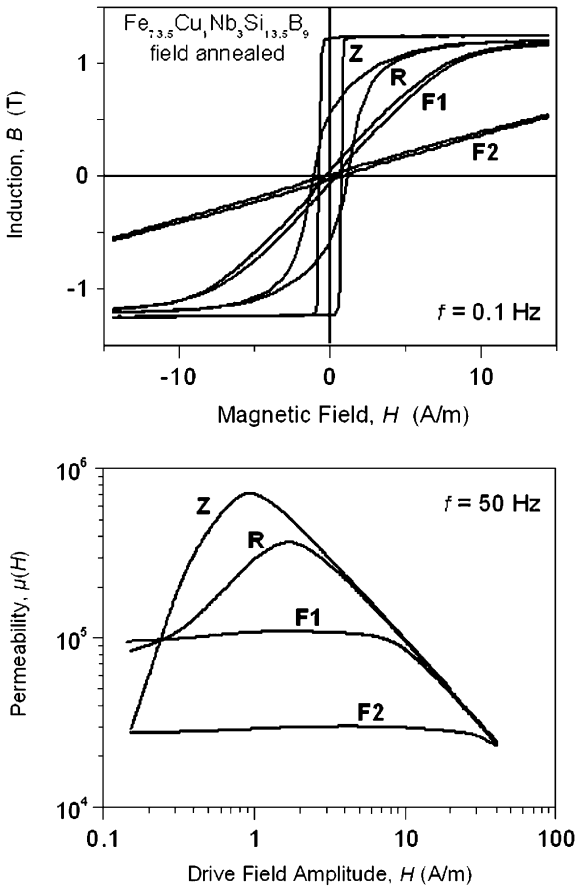

Fig. 3. Quasistatic hysteresis loops and 50 Hz permeability of nanocrystalline $Fe_{73.5}Cu_1Nb_3Si_{13.5}B_9$ annealed for 1 h at 540 °C without (R) and with a magnetic field applied parallel (*Z*) and transverse (F2; $K_u \approx 20\,J/m^3$, $\mu \approx 30 \times 10^3$) to the magnetic path. Sample F1 ($K_u \approx 6\,J/m^3$, $\mu \approx 100 \times 10^3$) was first crystallized at 540 °C and subsequently transverse field annealed at 350 °C (cf. [3]).

by field induced anisotropies, there are still situations where the random magneto-crystalline anisotropy becomes significant.

The most well-known example is the temperature dependence of the soft magnetic properties. The reason is that the exchange interaction between the nanocrystalline grains is largely reduced when the temperature approaches the Curie temperature of the amorphous matrix [2,3]. As a consequence the random magneto-crystalline anisotropy is less effectively averaged out and, hence, its average magnitude increases with increasing temperature.

Fig. 4 shows the typical temperature dependence of the remanence magnetization and of coercivity as found for transverse field annealed samples. Below T_c^{am}, the linear shape of the hysteresis loop and the low remanence clearly indicate that the field induced anisotropy dominates over the random anisotropies. Above T_c^{am}, however, the increase of both coercivity and remanence to saturation ratio reflect the increasing and finally dominating contribution of the random magneto-crystalline anisotropy.

Fig. 5 gives another example for the competition of random and uniform anisotropies at room temperature. In this case, the contribution of the random anisotropy is approximately constant and the strength of field induced anisotropy is varied.

The increase in the remanence to saturation ratio below induced anisotropies of about $K_u \approx 2$–$4\,J/m^3$ indicates the point where the random anisotropies start to dominate. Recent investigations [11] show that samples with such weak induced anisotropy K_u reveal irregular magnetization patches within the wide regular domains oriented along the induced anisotropy.

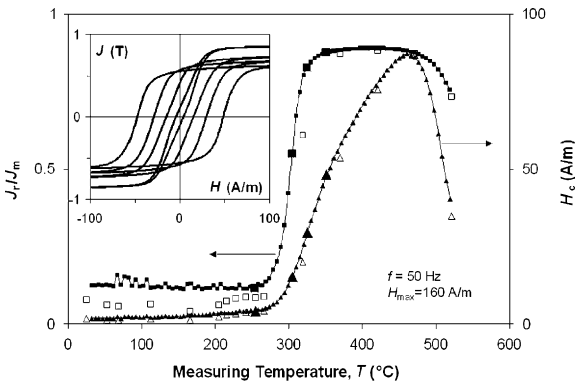

Fig. 4. Temperature dependence of remanence to saturation ratio, J_r/J_m, and coercivity, H_c, of nanocrystalline $Fe_{72.5}Cu_1Nb_3Si_{17.5}B_7$ annealed for 30 min at 540 °C in a transverse magnetic field. The induced anisotropy at room temperature is $K_u \approx 7\,J/m^3$. The inset shows the hysteresis loops at temperatures of 260, 300, 320 and 350 °C, respectively, which are highlighted by the enlarged symbols. The behavior is largely reversible upon heating (open symbols) and cooling (filled symbols).

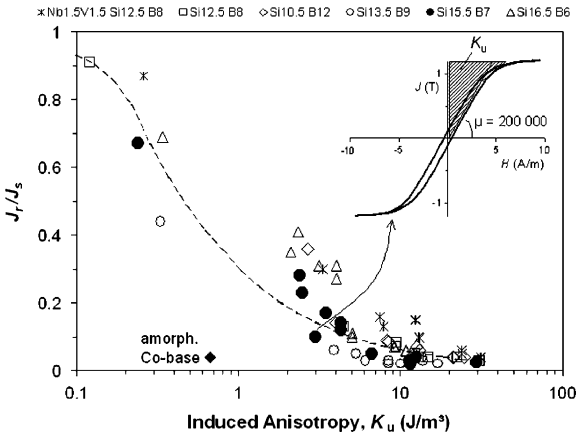

Fig. 5. Remanence to saturation ratio, J_r/J_m, of nanocrystalline $Fe_{bal}Cu_1Nb_3Si_xB_y$ alloys as a function of the field-induced anisotropy K_u. The samples were first crystallized for 1 h at 540 °C and subsequently transverse field annealed between 350 and 540 °C in order to vary K_u. For comparison, the figure also shows the result for an amorphous $Co_{67}Fe_4Mo_2Si_{16}B_{11}$ alloy (VITROVAC® 6025F) with a small transverse field-induced anisotropy of $K_u \approx 0.6\,J/m^3$.

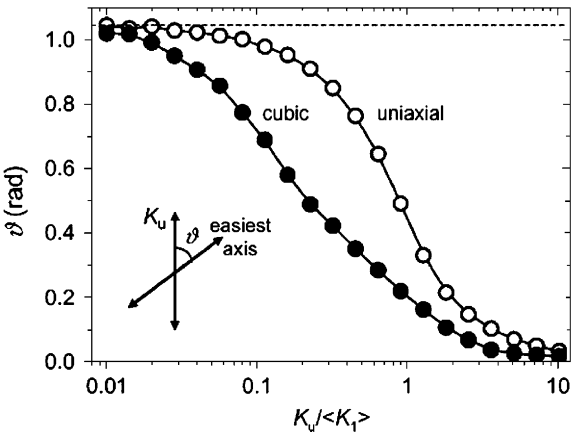

Fig. 6. Average orientation ϑ of the easiest magnetic axis for a system of randomly oriented particles with average anisotropy constant $\langle K_1\rangle$ and a superimposed, uniform uniaxial anisotropy K_u (full symbols: randomly oriented cubic grains; open symbols: uniaxial grains, dashed line: limit for $K_u = 0$).

These magnetization patches are fluctuating on a scale of a few micrometers which is the order of the renormalized exchange length $L_{ex} = \varphi(A/\langle K\rangle)^{1/2}$. They reflect the angular dispersion of the easiest magnetic axis from one region of exchange coupled grains to the other.

In comparison, amorphous Co-based alloys still show a low remanence, a linear hysteresis loop and no comparable inhomogeneities of the domain pattern even for much smaller values of the field induced anisotropy. The reason is the much smaller average random anisotropy energy.

5. Theoretical results

Fig. 6 illustrates the competition of a uniform uniaxial anisotropy K_u and the average random anisotropy $\langle K_1\rangle$ as obtained by numerical simulations [12]. This theoretical result reflects qualitatively the experimental findings shown in Figs. 4 and 5. For small K_u the easiest magnetic axis is dominated by the random anisotropy. Accordingly, the easiest axis reveals a large angular dispersion from one region of exchange coupled grains to the other. In experiment, this is manifested in the aforementioned patchy magnetization fluctuations on the scale of the renormalized exchange length [11]. However, as K_u approaches and finally exceeds the average random anisotropy contribution $\langle K_1\rangle$, the easiest magnetic axis is rotated towards the macroscopic anisotropy axis and the angular dispersion of the easiest axis disappears more and more.

Fig. 7 illustrates the expected grain size dependence of the average random anisotropy for typical Fe-based nanocrystalline alloys. We, hereby, have included the contribution of the random atomic scale anisotropy of the amorphous matrix as well as the case of a small uniform anisotropy K_u. The calculation is based on a recent extension [12] of the random anisotropy model which is summarized in the appendix.

In the absence of long-range anisotropies, the average anisotropy $\langle K\rangle$ is scaling with D^6 down to grain sizes of about 5 nm. Although the atomic scale anisotropy of the amorphous phase may be almost two orders of magnitude higher than that of the BCC crystallites, its average contribution is virtually negligible in this regime since the structural anisotropies are fluctuating on the much shorter scale of atomic distances ($D_{am.} \approx 0.5$ nm).

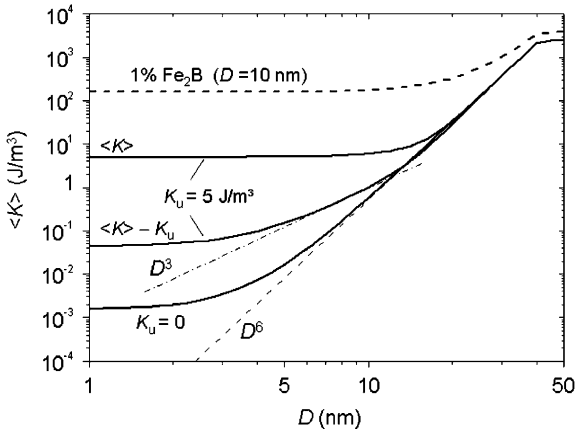

Fig. 7. Theoretical estimate of the average anisotropy $\langle K\rangle$ for a system of randomly oriented crystallites of BCC $Fe_{80}Si_{20}$ ($K_1 = 8.2\,kJ/m^3$) with grain size D and embedded in an amorphous matrix with a volume fraction $x = 0.75$. The atomic scale anisotropy constant of the amorphous phase was assumed as $K_1 = 430\,kJ/m^3$ which is the value for Fe_2B and which can be looked upon as an upper bound. Further material parameters are found in Ref. [12].

The random anisotropy of the amorphous matrix becomes only visible for very small grains resulting in a grain size independent anisotropy. However, the related coercivity ($H_c \sim 0.001\,A/m$) is so small, that the situation shown for smallest grain sizes in Fig. 7 remains academic. In real materials, whether amorphous or nanocrystalline, the minimum H_c is ultimately determined by more long range anisotropies.

The situation changes in the presence of a uniform anisotropy K_u. As can be seen from Fig. 7, the average anisotropy constant $\langle K\rangle$ is totally determined by K_u for grain sizes below about 10–15 nm. The contribution of the random anisotropies, i.e. $\delta K = \langle K\rangle - K_u$, simultaneously changes from a D^6-dependence to a D^3-dependence and, finally, gets grain size independent due to the random anisotropy of the amorphous phase. The latter is larger than for the case $K_u = 0$, because K_u limits the renormalized exchange length to a maximum value given by $L_{ex} = \varphi(A/K_u)^{1/2}$. As a consequence the random anisotropies are less effectively averaged out.

A very small volume fraction of a phase with high anisotropy can finally change the picture totally. This is illustrated in Fig. 7 assuming a 1% fraction of Fe_2B precipitates with 10 nm grain size. The example explains at least qualitatively the finding that Fe_2B precipitates can significantly deteriorate the soft magnetic properties although the grain size of the BCC crystallites remains unchanged (cf. Fig. 1).

For pure random anisotropies averaged out by exchange interaction, coercivity H_c and initial permeability μ_i are simply related to the average anisotropy constant by $H_c \propto \langle K\rangle$ and $\mu_i \propto 1/\langle K\rangle$, irrespective of the detailed magnetization process [2]. If we deal with additional more macroscopic anisotropies, however, the theoretical description of H_c and μ_i gets readily more complex like in conventional soft magnetic materials:

For domain wall displacements coercivity, H_c, is determined by the anisotropy fluctuations δK according to

$$H_c \approx \frac{1}{2J_s}\left|\frac{\partial \gamma_w}{\partial x}\right|_{max} \approx \frac{\delta K}{J_s}\frac{L_{ex}}{\lambda}, \tag{3}$$

where $\gamma_w = 4(A\langle K\rangle)^{1/2}$ is the domain wall energy, J_s the saturation magnetization, $L_{ex} = \varphi(A/\langle K\rangle)^{1/2}$ the renormalized exchange length and λ the fluctuation length of the anisotropy.

For exchange coupled grains, λ equals to the exchange length, i.e. $\lambda \approx L_{ex}$. The coercivity then is proportional to the random anisotropy dispersion δK. Hence, we expect that the grain size dependence of coercivity changes from D^6-dependence to a D^3-dependence as K_u starts to dominate (cf. [8]) and, finally, gets grain size independent at smallest grain sizes.

More long-range anisotropy fluctuations on a scale $\lambda > L_{ex}$ can of course contribute to H_c as well. This gives a grain size independent contribution, $H_c \propto K_u^{1/2}/\lambda$, which can dominate over the random microstructural anisotropies. This is the case in amorphous alloys and in nanocrystalline Fe–Cu–Nb–Si–B alloys for grain sizes below about $D < 10$–15 nm (cf. Fig. 1 and Ref. [8]).

Permeability μ behaves even more complex if we deal with superimposed long-range anisotropies. It depends sensitively on the angle between field and macroscopic anisotropy direction. If the sample is magnetized perpendicular to the K_u-axis, μ is inversely proportional to the total anisotropy,

i.e. $\mu \propto 1/\langle K\rangle$. It is, thus, grain size independent if K_u is dominating although coercivity may simultaneously vary proportional to D^3. If magnetized parallel to the uniform anisotropy axis μ is determined by domain wall pinning and we expect $\mu \propto 1/\delta K$.

6. Conclusions

For grain sizes $D < 15$ nm, the average random anisotropy in nanocrystalline Fe-based alloys is largely averaged out and the soft magnetic properties are increasingly controlled by uniaxial anisotropies which are uniform on a scale much larger than the exchange length. The most relevant contributions are magneto-elastic anisotropies and, most noticeably, field-induced anisotropies. Thus, if the grain size is sufficiently reduced, the general parameters for material optimization appear to be pretty much the same as in amorphous metals.

Yet, unlike to the case of soft magnetic amorphous alloys, there is still a competition between the random and uniform anisotropy contributions even in soft magnetically optimized nanocrystalline alloys. The achievable initial permeabilities are thus limited to values $\mu_i < 3 \times 10^5$. Another well-known example is the temperature dependence of the soft magnetic properties.

Appendix

We summarize here the conclusions of a recent extension of the random anisotropy model based on an analytical model calculation and numerical simulations [12].

Accordingly, the average anisotropy constant $\langle K\rangle$ of a *coupled* multi-phase system with anisotropies randomly oriented on a scale smaller than a magnetic correlation length L_{ex} can be well described by

$$\langle K\rangle = \sqrt{K_u^2 + \sum\nolimits_v x_v \beta_v^2 K_{1,v}^2 (D_v/L_{ex})^3}, \tag{A1}$$

where K_u denotes a uniaxial anisotropy which is *uniform* on a scale much larger than L_{ex}. The random contributions are represented by the local anisotropy constants $K_{1,v}$, the grain sizes D_v and the volume fractions x_v of the individual structural phases labeled by the index v. The parameters β_v mainly involve conventions used for defining the anisotropy constants for different symmetries, but also include some statistical corrections in the order of 10–20%. Numerical simulations for single phase systems result in $\beta \approx 1$ for uniaxial and $\beta \approx 0.4$ for cubic symmetry. $\langle K\rangle$ is defined as the difference between the maximum and minimum of the average anisotropy energy density. The result is valid as long as the average number of *coupled* grains $N_v = x_v(L_{ex}/D_v)^3$ is larger than one for each individual phase.

For the derivation of Eq. (A1) it is only necessary to assume that the magnetization is parallel within a volume defined by a correlation length L_{ex} without specifying the precise coupling mechanism.

If the coupling mechanism is dominated by *exchange interaction*, the correlation length L_{ex} is self-consistently related to the average anisotropy constant $\langle K\rangle$ by

$$L_{ex} = \varphi\sqrt{A/\langle K\rangle}. \tag{A2}$$

In the general case, the average anisotropy $\langle K\rangle$ has to be determined from Eqs. (A1) and (A2) by numerical iteration. Explicit solutions can be obtained in the limiting cases of a vanishing or dominating macroscopic anisotropy K_u. The results are

$$\langle K\rangle = \left(\sum_v x_v \sqrt{\beta_v |K_{1,v}|}(D_v/L_{0,v})^3\right)^2 \tag{A3}$$

for $K_u = 0$, and

$$\langle K\rangle \approx K_u + \frac{1}{2}\sum_v x_v \sqrt{\beta_v |K_{1,v}| K_u}(D_v/L_{0,v})^3 \tag{A4}$$

if the uniform anisotropy is dominating over the random contributions. In the above relations

$$L_{0,v} := \varphi_{0,v}\sqrt{A/|K_{1,v}|} \quad \text{with } \varphi_{0,v} := \varphi/\sqrt{\beta_v} \tag{A5}$$

define the *basic* exchange lengths related to the *local* anisotropies of the individual structural phases (cf. Eq. (1)). These length scales should not be confused with the *renormalized* exchange

length L_{ex} of Eq. (A2) which is self-consistently related to the *average* anisotropy $\langle K\rangle$. The prefactors φ_0 are expected to be about $\varphi_0 \sim 1.5$.

In the regime where the contribution of the BCC crystallites is dominating, the expression for $\langle K\rangle$ and simplifies drastically, i.e.

$$\langle K\rangle := \beta\langle K_1\rangle = \beta|K_1| \cdot x^2 (D/L_0)^6. \quad \text{(A6)}$$

The only modification compared to a single phase system is that the relations involve the crystalline volume fraction x.

References

[1] Y. Yoshizawa, S. Oguma, K. Yamauchi, J. Appl. Phys. 64 (1988) 6044.
[2] G. Herzer, IEEE Trans. Magn. 25 (1989) 3327; G. Herzer, IEEE Trans. Magn. 26 (1990) 1397.
[3] G. Herzer, Nanocrystalline soft magnetic alloys, in: K.H.J. Buschow (Ed.), Handbook of Magnetic Materials, vol. 10, Elsevier, Amsterdam, 1997, p. 415.
[4] Y. Yoshizawa, K. Yamauchi, IEEE Trans. Magn. 25 (1989) 3324.
[5] Vacuumschmelze GmbH, Toroidal Cores of VITROPERM, Data Sheet PW-014, 1993.
[6] J. Petzold, J. Magn. Magn. Mater. 242–245 (2002) 84.
[7] R. Alben, J.J. Becker, M.C. Chi, J. Appl. Phys. 49 (1978) 1653.
[8] K. Suzuki, G. Herzer, J.M. Cadogan, J. Magn. Magn. Mater. 177–181 (1998) 949.
[9] R. Grössinger, R. Sato, H. Davies, this Workshop.
[10] R. Schäfer, A. Hubert, G. Herzer, J. Appl. Phys. 69 (1991) 5325.
[11] S. Flohrer, R. Schäfer, C. Polak, G. Herzer, Acta Mater., 2005, in press (accepted 4 March 2005, available online 9 April 2005).
[12] G. Herzer, The random anisotropy model, in: B. Idzikowski, P. Švec, M. Miglierini (Eds.), NATO Science Series II: Mathematics, Physics and Chemistry, vol. 184, Kluwer Academic, Dordrecht, 2005, p. 15.